J. Fluid Mech. (2006), *vol.* 555, *pp.* 113–130.
doi:10.1017/S0022112006008780 Printed in the United Kingdom

Interaction and collisions between particles in a linear shear flow near a wall at low Reynolds number

By PIETRO POESIO[1], GIJS OOMS[1], ANDREAS TEN CATE[2] AND JULIAN C. R. HUNT[1,3]

[1]J.M. Burgers Center, Delft University of Technology, Laboratory for Aero- and Hydrodynamics, Leeghwaterstraat 21, 2628 CA Delft, The Netherlands

[2]Chemical Engineering Department, Engineering Quadrangle, Princeton University, Princeton, NJ, USA

[3]Department of Space and Climate Physics, University College London, Gower Street, London WC1E 6BT, UK

(Received 5 May 2004 and in revised form 26 October 2005)

The flow field around pairs of small particles moving and rotating in a shear flow close to a wall at low but finite Reynolds number (Re) is computed as a function of time by means of the lattice-Boltzmann technique. The total force and torque acting on each particle is computed at each time step and the position of the particles is updated. By considering the lift force and the disturbances induced by the particles, the trajectories of the pair of particles are explained as a function of the distances from the wall and the Reynolds number. It is shown that when particles are positioned in a particular form, they collide forming strings. In particular, we are interested in particle-bridge formation in shear flows, and two collided particles (a string) can be considered as a nucleus of a particle bridge.

1. Introduction

Clustering of small particles in a laminar or turbulent flow field occurs often in practice. In the clustering process, hydrodynamic forces are dominant, but colloidal forces play an important role. We are particularly interested in the clustering of particles in the pores of a porous material because the particles can form bridges in the throat of the pores and reduce the permeability of the material. An example is given in figure 1, where bridge formation by very small particles in a natural sandstone is shown; note that their size is less than 1/100 of the pore diameter. This type of fouling can cause severe problems during the exploitation of oil from an underground reservoir and it is important to understand better under which conditions bridge formation by particles can occur. During the movement of the particles through the pore of a porous material the Reynolds number is very low (10^{-3}–10^{-2}). Another important characteristic is that there is always a solid wall not far away from the particles. As the study of how particles form bridges is complicated, we begin studying the flow of a single particle in the vicinity of a wall. To that purpose the flow field around the particle is computed as a function of time by means of the lattice-Boltzmann technique (ten Cate 2002; ten Cate *et al.* 2002). The total force and torque acting on the particle is computed at each time step and its position is updated. The trajectory and the particle induced disturbance are studied as a function of the distance from the wall and for different Re. Next we extend the study by investigating the behaviour of two

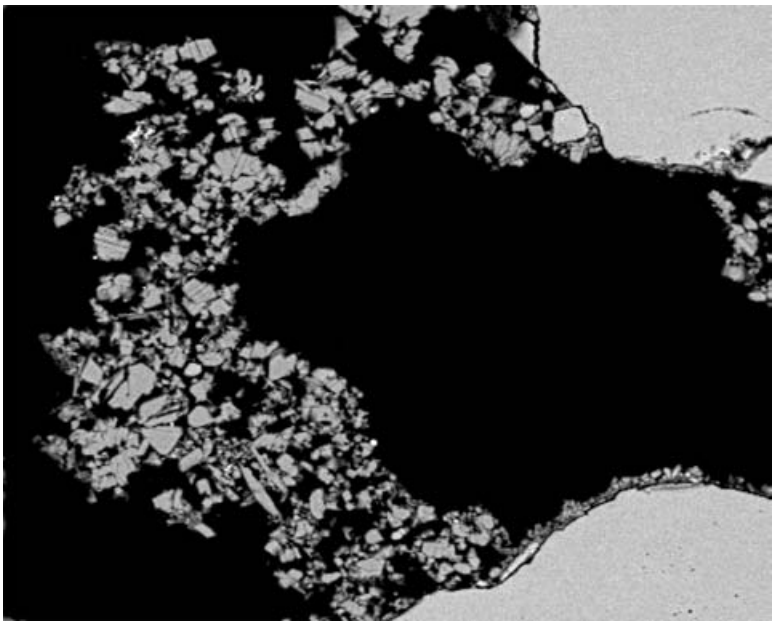

FIGURE 1. Particles bridge formation in a pore throat inside a natural sandstone. Note that particles have a variety of sizes.

particles. Particular attention is paid to the possibility that the particles collide and form the nucleus of a string of particles. In the final part of the paper, the possibility that two particles form a bridge in a converging flow configuration is investigated.

Several papers have been written about the hydrodynamic forces acting on a particle travelling in a shear flow at low, but finite, Reynolds number. The first to compute the inertial lift force on a spherical particle moving in such a shear flow was Saffman (1965). Cherukat & McLaughlin (1994) computed the lift force acting on a spherical particle near a wall by means of a perturbation approach. Magnaudet (2003) calculated the drag force and the lift force on a sphere in a linear shear flow near a wall. Feng & Michaelides (2003) studied numerically the motion of a single particle near a horizontal wall in a linear shear flow. They investigated at which conditions the inertial lift force acting on a particle is large enough to overcome the gravity force, allowing the particle to move away from the wall. As the finite size of the particle is taken into account, the disturbance of the particle on the flow field is also calculated. The lift force on a rotating sphere in a shear flow was studied by Kurose & Komori (1999); they showed that, at high Re, the lift force changes orientation. Kurose & Komori (1999) computed the hydrodynamic forces acting on a spherical particle held in place with an imposed rotational speed, whereas we are interested in the case where the motion of the particle is driven by the flow. Patankar *et al.* (2002) studied the lift-off of a sphere in a two-dimensional channel by means of direct numerical simulations. They paid particular attention to the role of the lift force for relatively high Re with the influence of gravity.

When two particles are moving in a shear flow close to a wall, it is not immediately clear in which direction they will move. For instance, it is possible that the trailing particle moves toward the wall owing to the flow disturbance of the leading particle, while the leading particle itself moves away from the wall owing to the inertial lift force. It is also possible that both particles move away from the wall because the

inertial lift force dominates the movements of the particles. There is competition between the viscous force and inertial force acting on the particles and at low, but finite, Re it is not clear which one dominates. The understanding of the behaviour of two interacting and colliding particle in a shear flow is fundamental to understanding the formation of particle clusters (for instance in the form of strings) and particle bridges in such flows. Sharp & Adrian (2001) reported about shear induced arching (called in our paper, bridging) to be the main mechanism causing channel blockage in microtubes. They drew this conclusion based on the observation of the geometrical configuration of the blockages; these blockages look very similar to the one we report in figure 1. The explanation is based on the likelihood of particles colliding when placed in a non-uniform laminar-flow velocity profile. Collisions are then followed by the formation of arches; they assume that 'particles are uniformly dispersed at the inlet of the channel, some mechanisms must bring the particles together in the channel', (see Yamaguchi & Adrian 2004). We show in this paper that this mechanism is correlated with a weak (but not negligible) inertial effect in the proximity of a wall.

In the formation of particle clusters or bridges, colloidal forces (for instance van der Waals forces or the electrical-double-layer force) can play a crucial role. The particles can be pushed together by hydrodynamic forces and particle cluster formation or particle bridge formation can then occur owing to the colloidal forces. Here, we limit ourselves (as a starting point) to the hydrodynamic interaction between two particles in a shear flow in the vicinity of a wall. Colloidal forces are taken into account in an indirect way. From the colloidal properties of the material (assumed to be clays) we can calculate at what distance the colloidal forces start playing a role. When the two particles become closer than this distance, we stopped the simulation and we recorded a 'collision'. Also, the flow geometry is first simplified by studying the flow of two particles in the shear flow close to a plane wall. In the last part of the paper, we investigate the movement and collision of particles in a convergent flow geometry, similar to that shown in figure 1. In such a way, first we understand the basic feature of particle collisions in a simplified geometry and later we will make use of this understanding to explain particle collisions and, hence, bridge formation in a more realistic, and more complex, geometry.

The practical and the environmental relevance of this study is discussed in the conclusion.

2. Lattice-Boltzmann method

2.1. *Numerical scheme*

For our numerical simulations, the lattice-Boltzmann method was used. This method can treat moving boundaries with a complex geometry in an efficient way. Simulations with this method for the case of a single spherical particle settling in a confined geometry have shown very good agreement with experimental results (see ten Cate 2002; ten Cate *et al.* 2002). The lattice-Boltzmann method uses a mesoscopic model for the fluid behaviour, which is based on collision rules for the movement of hypothetical particles (not to be confused with the physical particles) on a grid. The grid is a uniform simple cubic lattice. It can be shown that, after averaging, the continuity equation and Navier–Stokes equation are satisfied. The lattice-Boltzmann method was applied by Ladd (1994*a*, *b*) to calculate a flow with particles. Our method is based on the work of Eggels & Somers (1995); it is described in detail in ten Cate (2002). The boundary condition at the surface of a particle is taken into account by means of an induced force-field method, similar to that used by Derksen & van den

Akker (1999). In this method a particle is represented by a number of points located on its surface. The surface points are evenly distributed with a mutual distance smaller than the grid spacing. The no-slip condition at the particle surface is satisfied in two steps. First, the fluid velocity at each surface point is determined via a first-order interpolation of the fluid velocities in the surrounding grid points. Then (induced) forces are assumed to be present at the surface points of the particle, of such a magnitude that the fluid velocity in the surrounding grid points is changed in such a way that the no-slip condition at the surface points is satisfied. Thereafter, the hydrodynamic drag force ($\boldsymbol{F}_d$) and also the torque ($\boldsymbol{M}_d$) acting on a particle by the fluid are computed and used to determine the particle motion. The particle movement is calculated with the aid of the following equations

$$m\frac{\mathrm{d}^2\boldsymbol{x}}{\mathrm{d}t^2} = \boldsymbol{F}_d, \tag{2.1}$$

$$I\frac{\mathrm{d}^2\boldsymbol{\theta}}{\mathrm{d}t^2} = \boldsymbol{M}_d, \tag{2.2}$$

in which m is the particle mass, I the moment of inertia, $\boldsymbol{x}$ the space coordinate, θ the angle of rotation and t the time. This equation is integrated by using a simple Euler integration scheme where the forces are time-smoothed over two time steps.

The computations were carried out on a three-dimensional grid. We used particles of 10 lattice units (l.u.) radius. The length of the calculation domain is 400 l.u., the height is 400 l.u. and the perpendicular direction has a length of 200 l.u. In a few cases, we doubled the mesh size in each direction to investigate whether the results are independent of mesh size.

2.2. *Calibration procedure for the particle radius*

As discussed, a particle surface is approximated in the lattice grid by means of particle surface points. It is known that this approximation causes the particle to experience a drag force that corresponds to a particle with a diameter larger than the real diameter. This effect can be compensated by ascribing to the particle a hydrodynamic radius that is smaller than the real radius. For the determination of this hydrodynamic radius, a calibration procedure is applied. A now well-known procedure was proposed by Ladd (1994*a*). He calculated the drag force acting on a particle located in an array of particles with a periodic arrangement in two ways. He used his lattice-Boltzmann method and applied the analytical solution for this particular problem. From the comparison between the two results he found the hydrodynamic radius. The calibration procedure is based on the analytical solution of Hasimoto (1959) for the drag force on a fixed sphere in a periodic array of spheres at creeping flow conditions

$$\frac{6\pi\mu a U_u}{F_d} = 1 - 1.7601C_\tau^{1/3} + C_\tau - 1.5593C_\tau^2, \tag{2.3}$$

where $C_\tau = 4\pi a^3/3L^3$; L indicates the size of the unit cell, U_u is the volumetric averaged fluid velocity across the unit cell, μ the fluid viscosity and a the particle radius. We used the same calibration procedure.

The hydrodynamic radius was found for creeping flow conditions and we may wonder whether the result also holds at finite Reynolds number when inertial effects are important. Therefore, we have computed the inertial lift force on a sphere held stationary in a linear shear flow in the presence of a wall at low, but finite, Reynolds number. The results are compared with the analytical solution by Cherukat &

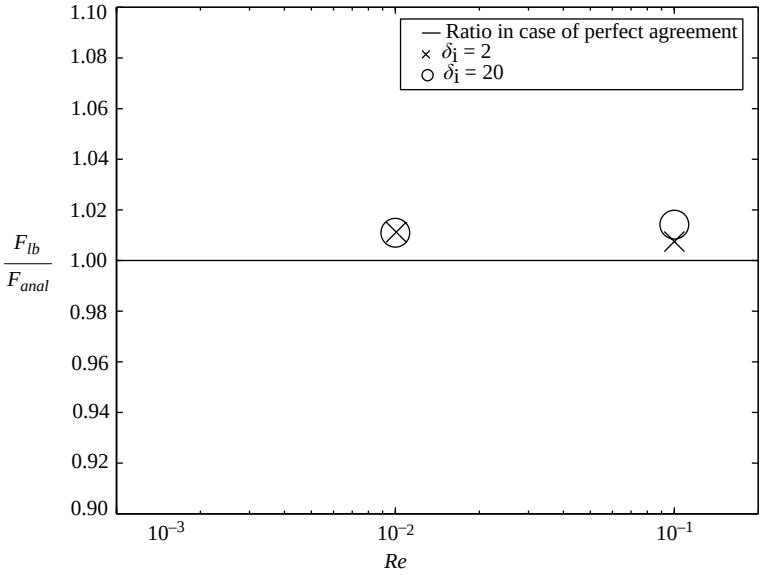

FIGURE 2. Comparison between the lift force on a particle as calculated by our method (F_{lb}) and as calculated analytically F_{anal} by the procedure given in Cherukat & McLaughlin (1994).

McLaughlin (1994) in figure 2 for two values of the dimensionless distance δ_i from the wall. ($\delta_i = y_i/a$, in which y_i is the distance from the wall and, as mentioned earlier, a the particle radius.) As can be seen, the results compare well.

2.3. *Lubrication force between two particles at a small distance*

Ladd (1997) found that for approaching particles, the lattice-Boltzmann method breaks down at very small distances between two particles owing to the lack of spatial resolution in the gap between the particles. He solved this problem by introducing an extra lubrication force that accounts for the contribution to the hydrodynamic forces due to the unresolved part of the flow field. This lubrication force (acting along the centreline of two particles i and j) is given by

$$\boldsymbol{F}_{lub} = -\frac{3\pi\mu a}{s}\hat{\boldsymbol{x}}_{ij}\hat{\boldsymbol{x}}_{ij}\cdot(\boldsymbol{u}_i - \boldsymbol{u}_j), \tag{2.4}$$

where $s = R/a - 2$ is the dimensionless gap width (R is the distance between the centres of the particles) and $\boldsymbol{x}_{ij} = \boldsymbol{x}_i - \boldsymbol{x}_j \cdot \boldsymbol{x}_i$ and $\boldsymbol{x}_j$ are the coordinates of the particles and $\hat{\boldsymbol{x}}_{ij} = \boldsymbol{x}_{ij}/|\boldsymbol{x}_{ij}|$; $\boldsymbol{u}_i$ and $\boldsymbol{u}_j$ are the particle velocities. The lubrication force is assumed to be active, when the gap width between two particles is smaller than the distance between two lattice grid points. As the near field hydrodynamic force plays a critical role in our simulation, we used an improved version for the lubrication force given by Kim & Karilla (1991), in which a logarithmic correction is included

$$\boldsymbol{F}_{lub} = -\left(\frac{3\pi\mu a}{s} + \frac{27\pi\mu a}{20}\log\frac{1}{s}\right)\hat{\boldsymbol{x}}_{ij}\hat{\boldsymbol{x}}_{ij}\cdot(\boldsymbol{u}_i - \boldsymbol{u}_j). \tag{2.5}$$

3. Relevant parameters

The particles are released with an initial velocity $U_p(t=0)$ equal to the unperturbed local fluid velocity, given by $U_0 = \alpha y_i$; α is the shear rate. The instantaneous particle

velocity is defined as $\boldsymbol{W}_p = (U_p, V_p) = \mathrm{d}\boldsymbol{x}_p/\mathrm{d}t$ and, hence, the relative horizontal velocity is $\Delta U_p = U_p - U_0(y_p)$ while the relative vertical velocity is $\Delta V_p = V_p$. The important parameters for our problem are the particle Reynolds number (Re)

$$Re = \frac{\rho_f a \sqrt{\Delta U_p^2 + \Delta V_p^2}}{\mu}, \tag{3.1}$$

and the shear flow number

$$S = \frac{\alpha a}{\sqrt{\Delta U_p^2 + \Delta V_p^2}}, \tag{3.2}$$

where ρ_f is the density of the fluid and (as mentioned earlier) μ is the fluid viscosity.

Since $Re = 0$ and $S \to \infty$ at $t = 0$, we introduce two alternative dimensionless groups: the shear Re_s-number,

$$Re_s = \frac{\rho_f a^2 \alpha}{\mu}, \tag{3.3}$$

and the initial dimensionless distance from the wall,

$$\delta_i = \frac{y_i}{a}. \tag{3.4}$$

We made calculations for the following two values of the shear Reynolds number $Re_s = 0.01$ and $Re_s = 0.1$. For the initial dimensionless distance from the wall for the leading particle, we chose $\delta_i = 20$ (particle far away from the wall) and $\delta_i = 2$ (particle close to the wall). The initial position of the trailing particle relative to the leading one is of crucial importance for the behaviour of the two particles and it is studied in detail.

4. Single particle in a linear shear field

A spherical particle in a shear field at non-zero Reynolds number undergoes both a drag force and a lift force. The effect of these forces is to move the particle away from the wall. Initially, the particle is released at a distance δ_i from the wall with the same velocity as the fluid. The particle begins to rotate, leading to a lift force that causes the particle to move away from the wall. Then, the difference in velocity between the fluid and the particle generates the drag force. It is known that the inertial lift force is proportional to the Reynolds number. As in our case the Reynolds number is small, only a small movement away from the wall is observed. After an initial period during which the initial conditions play a role, the particle trajectory becomes linear. Similar results have been found by Feng & Michaelides (2003) (at higher Reynolds number and with gravity effect). Calculations concerning the motion of a single particle in a shear flow were also performed by Patankar *et al.* (2002). They studied the lift-off of a single particle in a two-dimensional channel. Even if their conclusions and results are qualitatively similar to ours, it is worth pointing out that the shear Reynolds number they were interested in is much higher than ours. The relative velocity, defined as the fluid velocity at a certain position for the particle-free case minus the particle velocity at the same position, increases at the beginning and then becomes a constant value. The initial increase of the horizontal velocity is caused by the particle moving to regions where the fluid velocity is higher. The final relative velocity is very small (compared to the velocity of the unperturbed flow); the particle follows the fluid almost completely.

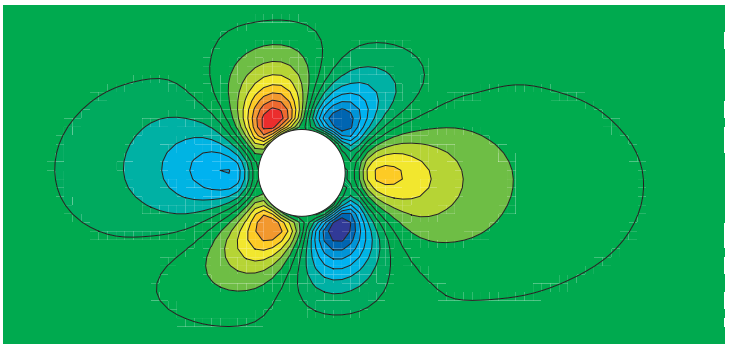

FIGURE 3. Plot of the vertical component of the fluid velocity. $Re_s = 0.01$ ($Re = 6.4 \times 10^{-4}$), initial position $\delta_i = 20$ and instantaneous position $\delta = 20.12$. Red: upward (positive component); blue: downward (negative component).

In order to understand the complicated flow field, we focus our attention on the vertical fluid velocity component, shown in figure 3. First, we consider the flow pattern around a single sphere moving in an unbounded fluid and then we discuss a particle moving in a shear flow without rotation and finally a rotating particle in a shear flow (without translation). In this way, the complete flow pattern around a particle moving in a shear flow with translation and rotation becomes clear.

The flow pattern around a single particle in a homogeneous flow can be found in many textbooks on fluid mechanics (see for instance Batchelor 1965). The asymmetry between the flow field at the back and at the front of the particle originates from the non-zero Re conditions (Oseen's flow). Next, we discuss the flow field for a particle translating in a linear shear without rotation. Of course, the particle has a tendency to start rotating, but we stopped this tendency. For a spherical particle in a shear flow, the two upper vertical-velocity lobes (that are positioned in the high-velocity region) are stronger than the two lower vertical-velocity lobes (that are in the low-velocity region). The asymmetry between the front of the particle and its back is due to the inertial forces at finite values of the Reynolds number and can also be observed for a particle in a homogeneous flow at non-zero values of the Reynolds number.

The vertical-velocity field around a rotating particle in a fluid (at rest at large distances) is determined by the fact that the fluid is dragged around to satisfy the no-slip condition.

We can now try to understand the fluid flow pattern shown in figure 3 in terms of the elementary 'building blocks' we have just described. Very close to the particle there is a thin layer of positive fluid vertical-velocity on the left-hand side of the particle, and a negative one on the right-hand side. These two regions are a consequence of the rotation of the particle in a clockwise direction. The two lobes at the top of the particle and the two lobes at the bottom are also because of the rotation of the particle, as can be concluded from their sign. So the rotation of the particle is very important in the determination of the fluid flow field. The two middle lobes originate from the two upper lobes for a translating non-rotating particle, but they are deformed because of the particle rotation.

We now analyse the forces acting on a particle using the fluid flow field around the particle, keeping in mind that ΔU_p and ΔV_p are horizontal and vertical relative velocities and Ω_p is the rotational speed. The force balance in the vertical direction must account for the upward inertial lift force ($\sim \rho_f \alpha a^3 \Delta U_p$), the downward force due to the Magnus effect ($\sim \rho_f \Omega_p \Delta U_p a^3$), and the component of the drag force in

the vertical downward direction ($\sim \mu a \Delta V_p$). An order of magnitude analysis shows that the inertial lift force and Magnus force are both significant, while the vertical component of the drag force is negligible. In the horizontal direction, there are two forces: the viscous drag ($\sim \mu a \Delta U_p$) (pointing forward as the particle travels slower than the fluid), and the horizontal component of the lift force ($\sim \rho_f \Omega_p \Delta V_p a^3$) (also pointing forward). Since $Re < 1$, the particle accelerates in the horizontal direction, as it rises in the shear flow.

The analysis of the flow field can now be used to understand the behaviour of a trailing second particle because, to the first approximation, the trailing particle behaves as a point particle without influencing the fluid. In the next section, this effect of the trailing particle is included. From figure 3, we see that a trailing particle responds to the flow field of the leading particle in a variety of ways. When the trailing particle enters the region behind the leading particle where the vertical velocity of the fluid is positive, the trailing particle has a tendency to be pushed upward. When the trailing particle enters the region where the vertical velocity of the fluid is negative, the trailing particle tends to move downward. However, there is an inertial lift force acting on the trailing and leading particles, that wants to push the particles upward. So while the leading particle will probably rise, the trailing particle can move upward or downward depending on the competition between the two tendencies described above. We comment on these suggestions in the next section where the results of two finite-size particles are presented.

We can also give a 'mechanism' diagram to explain the flow field around a particle in a shear flow and to explain the behaviour of a trailing second (point) particle (see figure 4). Again the flow field is considered to be built up from a number of basic elements. The flow disturbance due to the rotation of the particle is upward (u) on the left-hand side of the particle and downward (d) on the right-hand side (see figure 4*a*). Because of its inertia, the particle will move more slowly than the mean fluid velocity. This yields a flow disturbance with two recirculation regions, one above and one below the particle (see figure 4*b*). Finally, owing to the inertial lift force, the particle moves upward and causes also two recirculating regions, one at the left-hand side and one at the right-hand side of the particle (figure 4*c*). The combination of all contributions is sketched in figure 4(*d*). This diagram explains again, that a trailing second particle that enters the flow field behind the leading particle at a larger distance from the wall than the leading particle will probably move upward. A trailing second particle that enters the flow field behind the leading particle at a smaller distance from the wall than the leading particle will probably move downward.

The effect of Re on the vertical velocity of the fluid is analysed. The flow field is qualitatively the same as with the six lobes for the vertical component of the velocity. The fluid region around the particles that is influenced by the presence of the particles is reduced for larger values of the Reynolds number. This feature is essential for understanding the possibility of collision between the particles. At low values of the Reynolds number the presence of a particle is felt at larger distances from the particles than at high values. So at low values of the Reynolds number, the particles start feeling each other at larger distances (than for large values of the Reynolds number) and they have more time to rearrange their position.

The flow field around a particle is also influenced by the distance from the wall. As the particle becomes closer to the wall, the flow field close to the wall starts interacting with the wall itself. The region where the trailing particle is influenced by the leading particle is pushed upward and increases its size. The upper left lobe where the fluid is dragged upward, is pushed against the particle. We expect a collision to

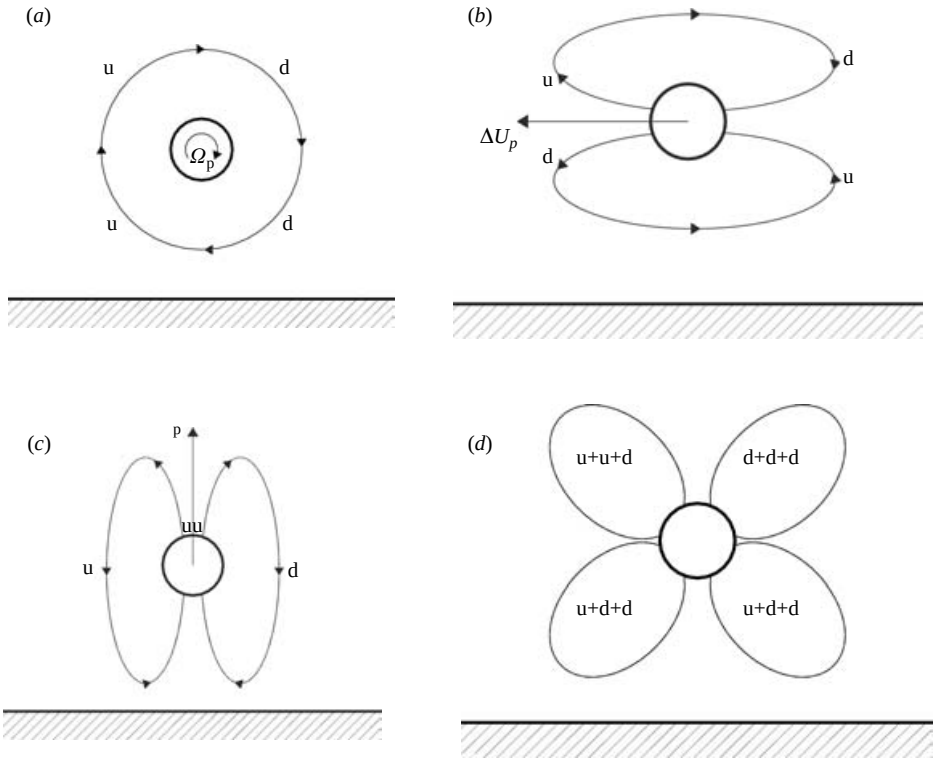

FIGURE 4. Mechanism diagram for flow field around a particle. u, upward; d, downward. (*a*) Particle spinning with angular velocity, Ω_p. $\Delta U_p = 0$, $\Delta V_p = 0$. (*b*) Particle translating horizontally with relative velocity ΔU_p. $\Delta V_p = 0$, $\Omega_p = 0$. (*c*) Particle translating vertically with relative velocity ΔV_p. $\Delta U_p = 0$, $\Omega_p = 0$. (*d*) Effect of the motion resulting from the superposition of (*a*), (*b*) and (*c*), showing that the dotted location is one that will continue and remain their.

be more likely for particles close to the wall than for particles far away from it. The trailing particle is not so easily pushed away from the leading particle as in the case where the particles are far away from the wall. The flow field is qualitatively similar in both cases, but a stronger interaction between the wall and particles close to the wall modifies more strongly both the size and the position of the six vertical-velocity lobes.

5. Two particles in a shear flow

We now study the hydrodynamic interaction and flow behaviour of two finite-size particles in a shear flow close to a wall at small, but finite, Reynolds number. So the fluid flow disturbance due to both particles is taken into account. Particular attention will be paid to the possibility of a collision between the particles. We study the interaction between two equal-size particles (with radius a) in a shear flow (with shear rate α). The particles are assumed to have initially the local fluid velocity and they are free to move and rotate in response to hydrodynamic forces. We can find two different types of trajectories for the particles. The trailing particle can first move downward toward the wall and move upward later on, or the trailing particle can move upward from the start. In both cases, the different behaviour is determined

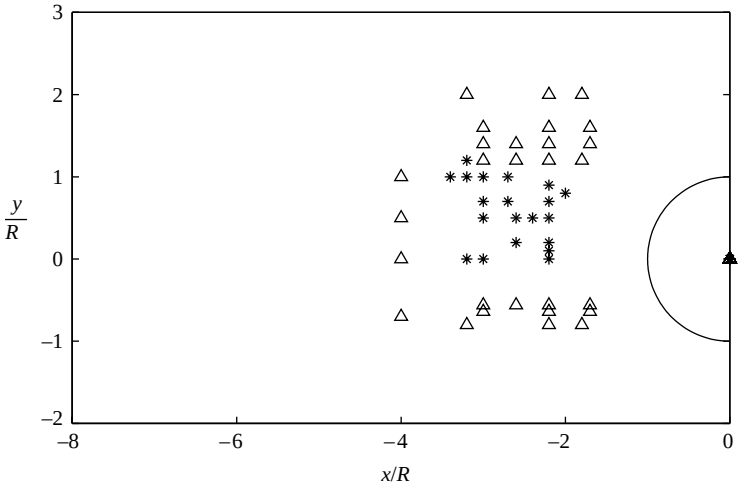

FIGURE 5. Trajectory map, giving an overview of the initial positions of the trailing particle with respect to the leading one. These lead to upward (△), i.e. moving away from the wall, or downward (∗), trajectories. $Re_s = 0.01$ and $\delta_i = 20$.

by the difference in the initial position of the trailing particle. If the trailing particle is initially completely immersed in a flow region of the leading particle where the fluid velocity is pointing downward, then it also starts moving downward. Whereas, if the trailing particle starts at a greater distance from the wall, where the influence of the leading particle pushes the particle upward, then it will move upward. So the conclusion is that when the particles are close together, the particle-induced fluid flow field dominates the particle relative movement. When the particles are farther apart, the shear flow field due to the presence of the wall becomes more important. When the particles do not collide, the distance between them increases and finally they behave as single particles and both move upward. In the final period also the velocity of the particles relative to the fluid is the same as in the case of a single particle. We do not treat here the case where the leading particle starts at a greater distance from the wall than the trailing one. In that case, the leading particle travels faster than the trailing one and it never catches up.

In the trajectory map (figure 5), we show the effect of the relative initial position on the initial stage of the trajectory of the trailing particle: a triangle means that, starting from that initial position, the particle initially move away from the wall, while an asterisk indicates particles initially moving toward the wall. As can be seen from the trajectory map, the region of initial positions for the trailing particles that initially move downward is not symmetrical behind the leading particle, the flow itself not being symmetrical. Note that the size of the region where these initially move downward shrinks as the Re increases. This is because the initial downward or upward bending of the trajectory of the trailing particle is induced by the movement of the leading particle and (as mentioned), at large values of the Re-number, this influence is less than at lower values. The leading particle will move upward regardless of the initial position of the trailing one because of the inertial lift force.

The flow pattern for two particles is similar to that for a single particle. The asymmetry in the vertical direction is a consequence of the shear field, the horizontal asymmetry is due to the inertial force at finite values of the Reynolds number. We want to analyse the flow pattern around the two particles. There is a strong interaction

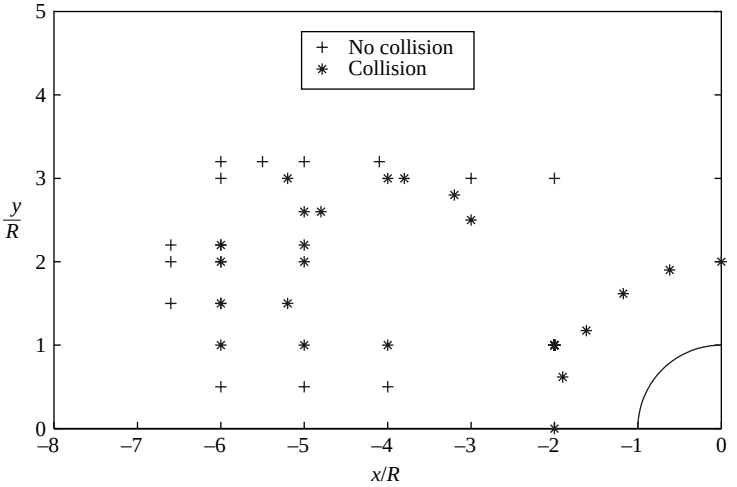

FIGURE 6. Collision map for $Re_s = 0.1$ and $\delta_i = 2$.

between the particles: the back region of the leading particle (where the vertical velocity component is pointing downward) influences the movement of the trailing particle. That region with a negative velocity component increases. Similarly, the region close to the leading particle that pushes the leading particle upward increases. These observations explain why, when the velocity regions completely overlap, the leading particle moves away from the wall faster than for the single-particle case, and also why the trailing particle initially moves downward. The interaction between the flow regions around the particles determines the trajectories of the particles and their possible collisions. It is worth noting that the vertical velocity component of the trailing particle is smaller than for the case of a single particle and this is due to interaction with the leading particle.

However, the situation is different when the negative vertical velocity region at the lower right-hand side of the trailing particle overlaps with the positive velocity region of the leading particle. The net effect is that the leading particle moves more slowly upward than for the single-particle case. The trailing particle moves upward more quickly than in case of a single particle. When this kind of flow pattern is observed, both particles will rise. In this case, the particles can rotate around each other and do not collide.

When the relative position is such that the lower right-hand velocity region of the trailing particle first interacts with the velocity region at the back of the leading particle, a collision does not take place. However, when the complete velocity region at the right-hand side of the trailing particle interacts with the velocity region at the back of the leading particle, a collision can occur. At high Reynolds number, the perturbed fluid velocity regions around the particles reduce in size.

To summarize the results we build the collision maps, sketched in figures 6 to 9. As discussed, the differences in flow pattern and particle trajectories depend on the way in which the two particles approach each other. The collision maps are made in the following way: we place the trailing particle at a certain initial position with respect to the leading particle, we release them with the local fluid velocity and we calculate the trajectories of both particles. We indicate on the collision map whether the initial positions of the two particles lead to a collision or not. So the map represents all the

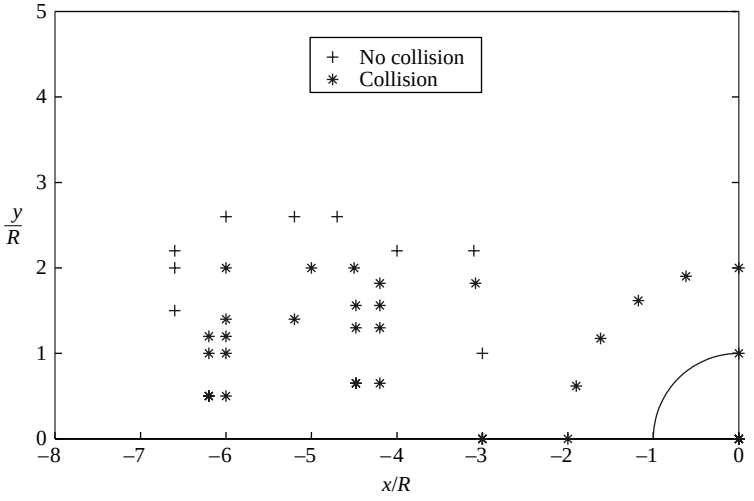

FIGURE 7. Collision map for $Re_s = 0.01$ and $\delta_i = 2$. As can be seen from a comparison with figure 6, the collision region decreases with decreasing Re_s-number.

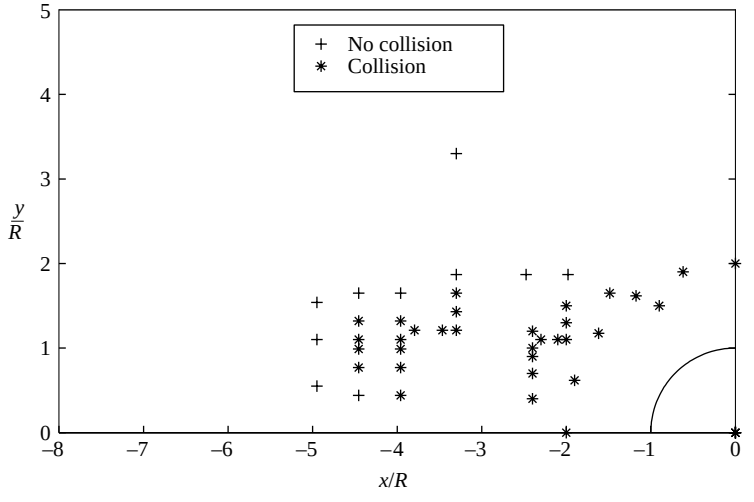

FIGURE 8. Collision map for $Re_s = 0.1$ and $\delta_i = 20$. As can be seen from a comparison with figure 6, the collision region decreases with increasing distance from the wall.

initial relative positions of the two particles that do or do not lead to a collision. This showed the influence of the initial positions on the likelihood of collisions.

We investigated the influence of the Reynolds number and the initial distance from the wall on the form of the collision map. The results are shown in figures 6 to 9. The influence of Reynolds number can be seen from a comparison between figures 6 and 7, and from a comparison between figures 8 and 9. The collision region increases with increasing Reynolds number. This is because the regions where the flow is disturbed reduce in size with increasing Reynolds number. The influence of the wall can be seen from a comparison between figures 6 and 8, and from a comparison between figures 7 and 9. As expected, more collisions will occur for particles close to the wall. This

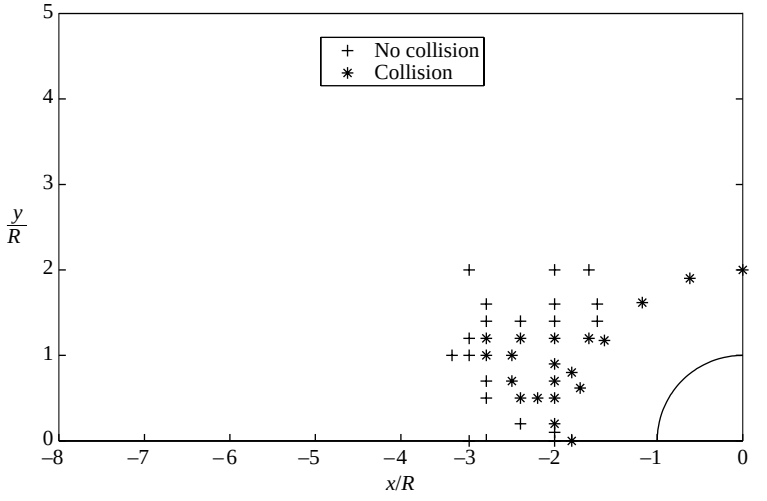

FIGURE 9. Collision map for $Re_s = 0.01$ and $\delta_i = 20$.

effect is due to the strong deformation of the flow field around the particles close to the wall, because the particle rotation is greater near the wall. The deformation region behind the leading particle, having a negative vertical component, increases and at the same time the wall pushes the leading particle away from it. As a result, more collisions occur. It can also be seen from the figures, that close to the wall the collision region is less influenced by the *Re*-number. So far, we have analysed only the case in which the initial positions of the two particles are in the same plane. It is interesting to look at possible effects of the offset in the out-of-plane direction. For the case $Re_s = 0.1$ and $\delta_i = 2$, we have carried out simulation for offsets (in the out-of-plane direction) equal to $a/4$, $a/2$, $3a/4$ and a. From figure 10, we can see similar collision maps to those shown before; it has to be noted that in this case the collision regions shrink so that for an out-of-plane offset equal to a, no collisions are found. We also simulated for the case at lower Re ($Re_s = 0.01$ and $\delta_i = 2$); qualitatively, the collision region is unchanged even if it shrinks more rapidly, as could be expected from previous discussions. The effect of the distance from the wall has been analysed by comparing the case at $Re_s = 0.01$ and $\delta_i = 2$ with the case at $Re_s = 0.01$ and $\delta_i = 20$. As the initial distance of the particles form the wall becomes greater, the collision region shrinks. In order to make a more quantitative description of the influence of the different parameters on the collision region, we have calculated the ratio between the area of the collision region and the particle surface as a function of the different parameters. These calculations are summarized in table 1. In the same table, we also show the volume of the collision region as a function of the different parameters.

We may wonder, what type of particle clusters may develop owing to collisions when many particles are present in the flow field. The results presented in the collision maps suggest that each particle tends to collide and cluster at the upper back part of a preceding particle.

6. Preliminary calculation of particle bridge formation

As mentioned in § 1 we are, in particular, interested in particle bridge formation in the pore throats of a porous material. To that purpose we have made a preliminary

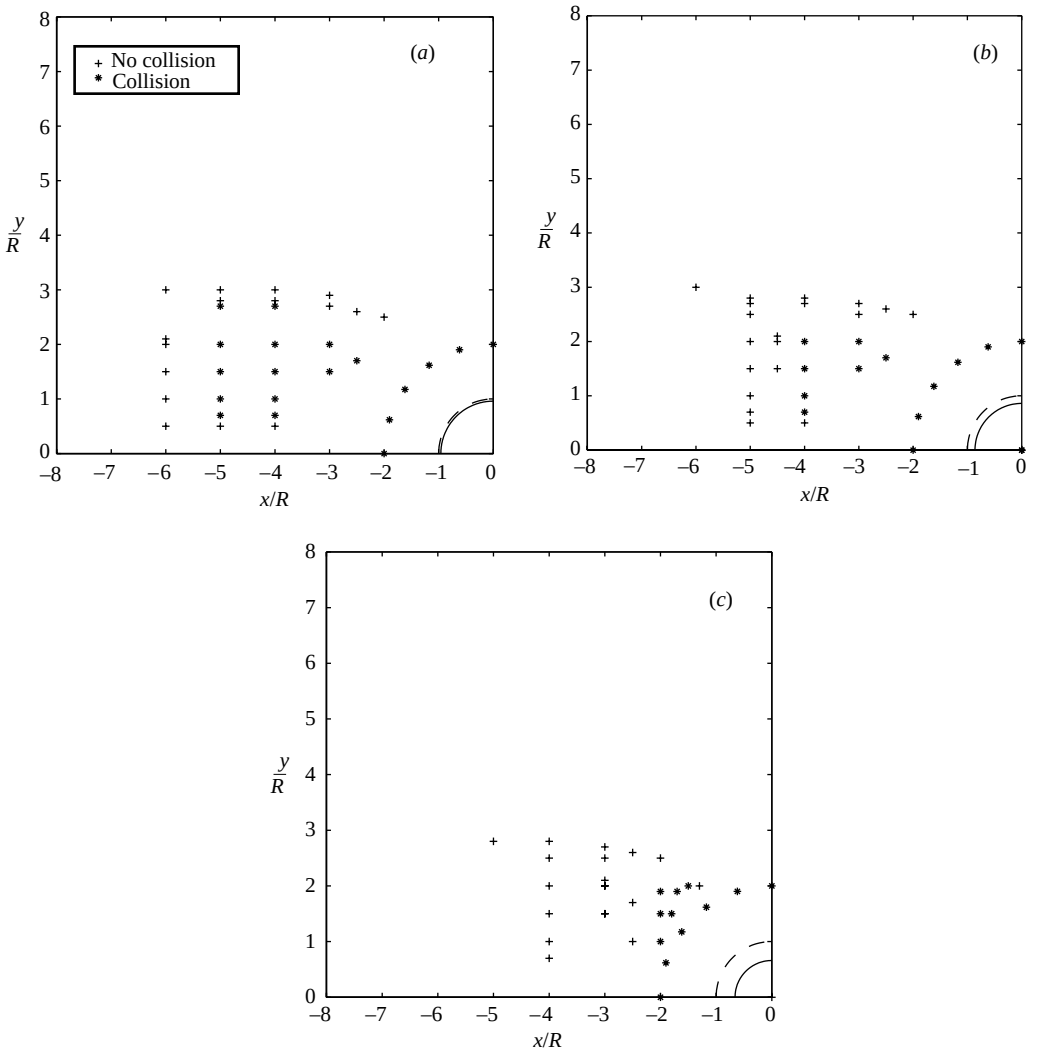

FIGURE 10. Influence of out-of-plane offset on the collision map for the case $Re_s = 0.1$ and $\delta_i = 2$. No collisions are recorded for an offset equal to a. (a) Collision map for $Re_s = 0.1$ and $\delta_i = 2$, the out-of-plane offset is $a/4$. The dotted line is the sphere of radius a, while the continuous line represents the sphere in the plane of the tralling particle. (b) Collision map for $Re_s = 0.1$ and $\delta_i = 2$, the out-of-plane offset is $a/2$. The dotted line is the sphere of radius a, while the continuous line represents the sphere in the plane of the trailing particle. (c) Collision map for $Re_s = 0.1$ and $\delta_i = 2$, the out-of-plane offset is $3a/4$. The dotted line is the sphere of radius a, while the continuous line represents the sphere in the plane of the trailing particle.

calculation concerning the movement, possible collision and bridge formation of two particles in a converging flow at the entrance to a (suddenly) narrowing part of a two-dimensional channel (the throat). In figure 11, a sketch of the flow geometry is given. For $x/a < 0$, there is a two-dimensional channel with solid walls at $y/a = -15$ and $y/a = +15$; for $x/a > 0$ the walls are at $y/a = -1.5$ and $y/a = +1.5$. Far upstream of the throat there is a parabolic fluid velocity profile, the flow is from left to right. Two particles can pass simultaneously through the throat only when they move behind

Out-of-plane offset	$Re = 0.01$ $\delta_i = 20$	$Re = 0.1$ $\delta_i = 20$	$Re = 0.01$ $\delta_i = 2$	$Re = 0.1$ $\delta_i = 2$
0	0.48	1.87	2.12	4.16
$a/4$	0.11	0.67	0.93	2.23
$a/2$	0	0.14	0.19	1.19
$3a/4$	–	0	0	0.44
a	–	–	–	0
Volume	0.12	0.71	0.93	1.43

TABLE 1. Collision areas (made dimensionless by πa^2) for different out-of-plane displacement as a function of the relevant parameters; the last line of the table shows the collision volume (made dimensionless by the $4/3\pi a^3$). The collision maps relative to those cases are available upon request.

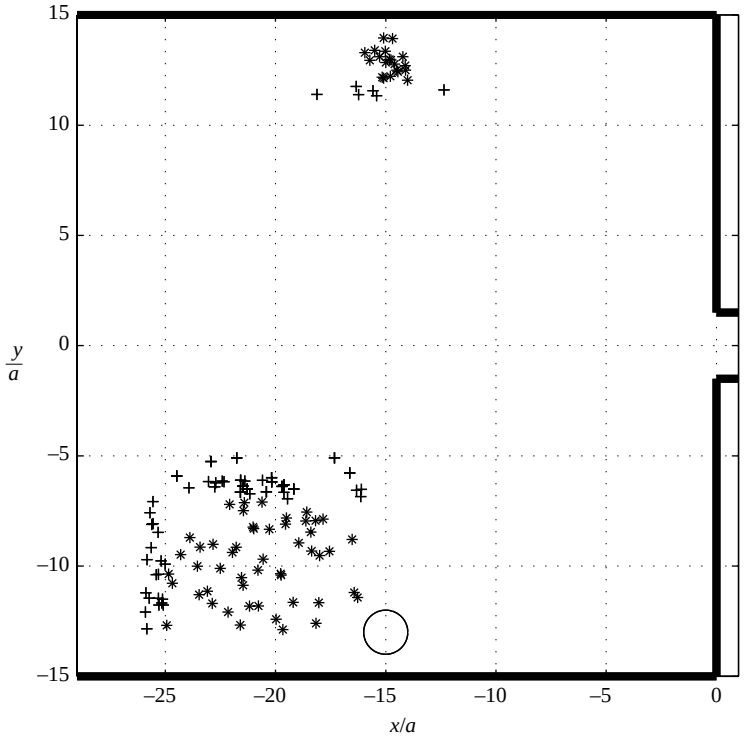

FIGURE 11. Bridge formation map for $Re_s = 0.01$ and $\delta_i = 20$. The initial position of the leading particle is at $x/a = -15$, $y/a = -13$. The bridge formation area is considerably larger than the collision area shown in figure 9. Moreover, it consists of two parts. The total collision area is $23.8a^2$. The same trend is noted for $Re_s = 0.1$, in this case the collision area is $29.2a^2$.

each other through the throat; in other cases, a particle bridge is formed at the throat entrance.

We have carried out additional lattice-Boltzmann calculation for two particles in the flow field with the geometry given in figure 11. The simulations are similar to those described in the preceding paragraphs for the movement of two particles in the vicinity of a flat solid wall, only the geometry is different. It is pointed out,

that although the geometry consists of a two-dimensional channel, the simulations are three-dimensional owing to the spherical geometry of the particles. In our simulations, we fixed the initial position of the leading particle at $x/a = -15$, $y/a = -13$, and we varied the initial position of the second particle. For all these cases, we calculated the trajectories of the particles and the possibility of a bridge formation by the two particles at the pore throat. We summarize the results in the bridge formation map also given in figure 11. As can be seen from figure 11, the bridge formation area (area of initial position of the second particle for which bridge formation occurs in the pore throat) is considerably larger than the collision area (area of initial position of the second particle for which collision occurs for the flow along a flat plate) shown in figure 9. Moreover, the bridge formation area consists of two parts. When the second particle starts in the vicinity of the wall on the opposite side of the pore, the two particles can arrive simultaneously at the pore throat. This is, of course, due to the converging flow close to the pore throat.

To investigate the influence of the inertia forces on the collision mechanisms and hence on bridge formation, we have carried out simulations at very low Re (i.e. $Re = 10^{-5}$). For this Re, we could not detect any collision apart from when the trailing particle starts at the symmetrical position. In this case, the collision is due to the (very unlike) starting position rather than to hydrodynamics effects. So, we believe that the inertia effect (even if small) is responsible of the collisions. To further stress this point, it is worth reminding that, for membranes, Ramachandran & Fogler (1998) experimentally found bridge formation appearing at $Re = 6 \times 10^{-3}$, but not at $Re = 1.2 \times 10^{-4}$. Poesio & Ooms (2004) reported bridge formation in porous media at low (but not zero) Re: bridge formation is reported to happen already at $Re = 10^{-3}$, but not at lower values. All the investigations reported so far have indicated a critical value of the Re at which particles start forming bridges and we believe this is connected with the increasing importance of the inertial forces. We are not able to predict this value, which depends on several flow features such as geometry, particle concentration and colloidal properties.

It is pointed out that much more work is required to study particle bridge formation in pore throats. For instance, in natural sandstones, bridge formation usually occurs with many particles (see figure 1). Three-dimensional simulations with so many particles are not possible at the moment.

7. Conclusion

In this study of the behaviour of two particles in a shear field in the vicinity of a wall, detailed computations and order of magnitude results have been presented for the flow disturbances around the particles. Particular emphasis is given to the conditions for which a collision between the particles occurs. To that purpose, collision maps have been calculated for two values of the Reynolds number and two values of the initial distance from the wall. In a collision map, the area of initial positions of the trailing particle with respect to the leading particle that leads to a collision, is shown. This collision area increases with increasing Reynolds number and decreasing distance of the leading particle to the wall. Also, a first investigation has been made of particle bridge formation in a converging flow geometry. It turns out that the likelihood of collision by particles and hence the bridge formation area for a converging flow is considerably larger than the collision area for the flow along a flat plate. We have shown that at very low Re ($Re = 10^{-5}$) collisions do not happen, while they appear at higher Re and they are more probable (i.e. they happen for a larger number of initial

positions) as *Re* increases. This indicates that, in proximity to the wall, collisions are dominated by weak inertia effects. This conclusion is in agreement with previous experimental works both on membranes (Ramachandran & Fogler 1998), and on natural porous material (Poesio & Ooms 2004). Of course, the particle shapes in reality may be different from the spherical one considered in this publication (see figure 1). However, as noted in the paper, the collision mechanism is dominated by the inertial lift force acting on the particles. It has been shown by Auton *et al.* (1988) that the lift force acting on a spherical-like particle in a shear flow is not sensitive to its precise shape.

This study relates to acoustic stimulation of fouled porous media. Decline in permeability has a very dramatic effect on the near wellbore region of an oil reservoir and it leads to a reduction in productivity. Many techniques have been used to overcome this problem (for instance the use of acid), but they have negative side effects (being, for instance, environmentally unfriendly). Recently, the acoustic stimulation of the near wellbore region has been proposed as a possible remedy. This technique is very cheap and environmentally friendly. The effectiveness of this technique is related to the cause of permeability reduction (particle deposition or particle bridge formation). While particle deposition is a widely known mechanism, formation of particle bridges was not understood. Poesio *et al*. (2004) have already studied the possibility of removing particles attached to the pore walls by acoustics. Experiments (Poesio & Ooms 2004), have shown that particle bridges can also be removed. Now that we have understood the phenomena involved in the bridge formation we are ready to take the next step and investigate the mechanisms involved in the removal of particle bridges.

REFERENCES

Auton, T. R., Hunt, J. C. R. & Prud'homme, M. 1988 The force exerted on a body in an inviscid unsteady non-uniform rotational flow. *J. Fluid Mech.* **197**, 241–257.

Batchelor, G. K. 1965 *An Introduction to Fluid Dynamics*. Cambridge University Press.

ten Cate, A. 2002 Turbulence and particle dynamics in dense crystal slurries. PhD thesis, Delft University of Technology.

ten Cate, A., Nieuwstad, C. H., Derksen, J. J. & van den Akker, H. E. A. 2002 PIV experiments and lattice-Boltzmann simulations on a single sphere settling under gravity. *Phys. Fluids* **14**, 4012.

Cherukat, P. & McLaughlin, J. B. 1994 The inertial lift on a rigid sphere in a linear shear flow field near a flat wall. *J. Fluid Mech.* **263**, 1–18.

Derksen, J. J. and van den Akker, H. E. A. 1999 Large eddy simulations on the flow driven by a Rushton turbine. *AIChE J.* **45**, 209–221.

Eggels, J. G. M., Somers, J. A. 1995 Numerical simulation of free convective flow using lattice-Boltzmann scheme. *Intl J. Heat Fluid Flow* **16**, 357–364.

Feng, Z.-G. & Michaelides, E. E. 2003 Equilibrium position for a particle in a horizontal shear flow. *Intl J. Multiphase Flow* **29**, 943–957.

Hasimoto, H. 1959 On the periodic fundamental solutions of the Stokes equations and their application to viscous flow past a cubic array of spheres. *J. Fluid Mech.* **5**, 317–328.

Ladd, A. J. C. 1994*a* Numerical simulation of particulate suspensions via a discretized Boltzmann equation. Part 1. Theoretical foundation. *J. Fluid Mech.* **271**, 271–309.

Ladd, A. J. C. 1994*b* Numerical simulation of particulate suspensions via a discretized Boltzmann equation. Part 2. Numerical results. *J. Fluid Mech.* **271**, 311–339.

Ladd, A. J. C. 1997 Sedimentation of homogeneous suspensions of non-Brownian spheres. *Phys. Fluids* **9**, 491–499.

Kim, S. & Karrila, S. J. 1991 *Microhydrodynamics*. Butterworth–Heinemann.

Kurose, R. & Komori, S. 1999 Drag and lift forces on a rotating sphere in a linear shear flow. *J. Fluid Mech.* **384**, 183–206.

Magnaudet, J. 2003 Small inertial effects on a spherical bubble, drop or particle moving near a wall in a time dependent linear flow. *J. Fluid Mech.* **484**, 167–196.

Patankar, N. A., Huang, P. Y., Ko, T. & Joseph, D. D. 2002 Lift-off of a single particle in Newtonian and viscoelastic fluids by direct numerical simulation. *J. Fluid Mech.* **445**, 67–100.

Poesio, P. & Ooms, G. 2004 Formation and ultrasonic removal of fouling particle structures in a natural porous material. *J. Petrol Sci. Engng* **45**, 159–178.

Poesio, P., Ooms G., van Dongen, M. E. H. & Smeulders, D. M. J. 2004 Removal of small particles from a porous material by ultrasonic irradiation. *Transport Porous Media* **54**, 239–364.

Ramachandran, V. & Fogler, H. S. 1998 Plugging by hydrodynamic bridging during flow of stable colloidal particles within cylindrical pores. *J. Fluid Mech.* **385**, 129–156.

Saffman, P. G. 1965 The lift on a small sphere in a slow shear flow. *J. Fluid Mech.* **22**, 385–400.

Sharp, K. V. & Adrian, R. J. 2001 Shear-induced arching of particle laden flows in microtubes. *ASME Intl Mech. Engng Congress and Exposition, vol. 3 New York, NY.*

Yamaguchi, E. & Adrian, R. J. 2004 Theoretical and Experimental Study of Microchannel Blockage Phenomena. *XXI ICTAM*, *Warsaw, Poland.*